

## Room temperature synthesis of high purity 2D ZnO nanoneedles

E. J. A. Campo<sup>a</sup>, M. Peiteado<sup>b,\*</sup>, A. C. Caballero<sup>b</sup>, M. Villegas<sup>b</sup>, J. E. Rodríguez-Páez.<sup>a</sup>

<sup>a</sup>Department of Physics-Group CYTEMAC, Universidad del Cauca, Popayán, Colombia.

<sup>b</sup>Department of Electroceramics, Instituto de Cerámica y Vidrio, CSIC, 28049 Madrid, Spain.

**Current technological requirements demand ZnO particles of controlled morphology, distribution and size. The achievement of such specific conditions cannot be guaranteed with conventional synthesis routes and new techniques should be applied to attain this goal. In the present contribution we prove that the controlled precipitation method (CPM) could be successfully applied to obtain high purity 2D zinc oxide nanoparticles with needle-type morphology. By using the appropriate precursors and washing medium, the synthesis could be achieved at room temperature without any additional thermal treatment required.**

**Key words:** ZnO, Nanostructures, Nanoneedles, Chemical synthesis.

### Introduction

Zinc oxide is an environmentally-friendly direct wide band-gap semiconductor (3.37 eV) with a large exciton binding energy and high mechanical and thermal stability. Nominally undoped ZnO forms in the hexagonal wurtzite-type crystal structure, with intrinsic defect levels leading to n-type doping. This makes zinc oxide an interesting material for its application in surface acoustic wave devices, piezoelectric transducers, varistors, gas-sensors, pigments, etc [1, 2]. As a wide bandgap semiconductor, ZnO is also a good candidate host for solid state blue to UV optoelectronics, including laser development, and for transparent high power electronics [3]. More recently the manipulation of spin in semiconductors (spintronics) has opened the door for new functionality in electronic materials, and ZnO offers a significant potential in providing charge, photonic, and spin-based functionality [4]. All these types of applications demand the use of high purity ZnO particles with controlled size and morphology, and this feature is even more critical when going to the nano scale. The physical and chemical properties of nanoparticles lead to novel and unique properties which are intrinsically associated with their low dimensionality and the quantum confinement effect [5]. Hence, according to the new technological requirements, the preparation of ZnO semiconductor nanostructures with a wide variety of morphologies has received broad attention in recent years [6-9]. Among these structures, two-dimensional ZnO nanostructures (2D) like nanorods and nanowires are especially attractive for their tuneable electronic and optoelectronic properties [10-13]. In addition semiconductor

nanoneedles are of particular interest, offering potential applications as probing tips with high spatial resolution, field-emission tips and reinforcement agents for elastomers [14, 15]. Although a fundamental description of the exact growth mechanism of nanostructures remains incomplete, various approaches have been employed successfully for the preparation of ZnO nanostructures. Preparation techniques include metal-organic chemical vapour deposition [16], hydrothermal synthesis with different precursors [17], pulsed laser deposition [18], thermal evaporation via a vapour liquid solid process assisted by a catalyst [19], oxidation of metallic Zn powder without a metal catalyst [5], crystallization from different precursors [20], etc. In previous studies we have applied the controlled precipitation method (CPM) to produce zinc oxide nanoparticles with different morphologies [15, 21]. By means of this method intermediate zinc complexes were formed during the precipitation process, and were partially transformed to zinc oxide after washing the initial colloidal suspension with ethanol. However when using acetate as a precursor of zinc, the washing step with ethanol does not complete the transformation to pure ZnO and additional thermal treatments are required, leading to undesirable agglomeration of the nanoparticles obtained [15]. In this new contribution we introduce modifications related to the precursors and the washing medium which allow the complete decomposition of zinc complexes during the washing stage. High purity 2D ZnO nanoparticles with a needle-like morphology are thus obtained without any thermal treatment by a simple chemical method.

### Experimental

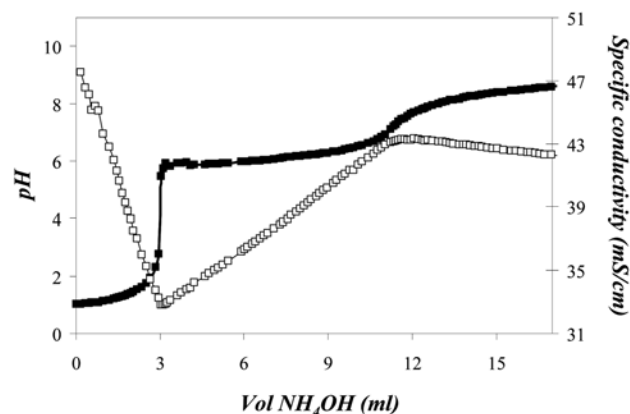
The room-temperature synthesis of ZnO nanoneedles was carried out by a controlled precipitation technique using an aqueous solution 0.34 M of zinc sulphate hepta-hydrated (Panreac) as precursor [21]. The solution was acidified

\*Corresponding author:  
Tel : +34-91-7355840  
Fax: +34-91-7355843  
E-mail: mpeiteado@icv.csic.es

to pH = 1 with nitric acid 0.1 M (Carlo Erba Reagenti), and then a solution 12 M of  $\text{NH}_4\text{OH}$  (Mallinkrodt 28.0-30.0%) was added gradually by 0.1 ml increments, using a Teflon capillary tube submerged below the solution-gas interface. During the addition of the precipitant, changes in pH and the specific conductivity were registered. The system was continuously stirred and the whole process was carried out at room temperature. The resulting precipitate was filtered and redispersed in a 0.03 M ethylenediamine solution using a high speed turbine (IKA T-50). The formation of ZnO in the solid during the washing stage is favoured by the shear action generated during the redispersion of the sediment when using the high speed turbine. This washing process was repeated up to eight times. After every washing, the samples were dried in a kiln at 80 °C for 2 days, ground in an agate mortar and characterized by X-Ray diffraction (XRD) using  $\text{CuK}\alpha$  radiation. In order to identify the surface groups formed during the process, infrared spectroscopy was carried out in a FT-IR Shimadzu spectrophotometer. The morphology of ZnO powders as well as the particle size was examined by transmission electron microscopy (TEM) on a JEOL 1200 EX microscope. The absence of impurities in the nanoneedles obtained was confirmed by energy-dispersive X-Ray spectroscopy (EDX).

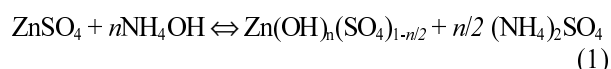
## Results and Discussion

Fig. 1 shows the potentiometric and conductimetric titration curves of the 0.34 M  $\text{ZnSO}_4$  aqueous solution. Three different zones can be distinguished in the potentiometric titration curve. The first zone is mainly affected by the presence of  $\text{HNO}_3$ , and it starts with a very slight and continuous increase in pH. This should be attributed to the low pH of the starting solution (pH ~ 1). However at the end of this zone I a pronounced increase in pH is observed which corresponds to the neutralization of the protons by  $\text{NH}_4\text{OH}$ . Once the neutralization is achieved (pH ~ 6) the curve enters into an extended quasi-horizontal plateau, zone II, which corresponds to an  $\text{OH}^-$  consuming

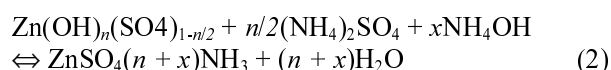


**Fig. 1.** Potentiometric and conductimetric titration curves of 0.34 M  $\text{Zn}(\text{SO}_4)$  aqueous solution.

process. After the plateau, a second increase in pH is observed in zone III until a constant value of pH = 8.6, when the solid precipitate is formed. The three zones detected in the potentiometric curve have their corresponding reflections in the conductimetric curve: three regions where the specific conductivity changes linearly with the volume of base added (Fig. 1). First in zone I, as long as the number of  $\text{H}^+$  is being reduced by the addition of ammonium hydroxide, the specific conductivity strongly decreases. Then the value of the conductivity increases in zone II due to the progressive formation of the different zinc sulphate complexes in the solution [21]. According to the following reaction such complexes are zinc basic sulphates:



Due to the excess of  $\text{NH}_4\text{OH}$ , dissolution of the above mentioned basic sulphates must take place then in zone III. This reaction can be written in the following way:



On the other hand ammonium hydroxide is a weak base and is poorly ionized. This explains why in zone III the specific conductivity finally reaches a saturation value at a high pH (Fig. 1).

Fig. 2 illustrates the FT-IR spectra of colloidal suspensions of the solid as obtained at pH = 8.6 and after being subjected to different washings with ethylenediamine. The main vibration modes and the assigned functional groups are also depicted in Table 1. The broad band around 3500-3200  $\text{cm}^{-1}$  includes the tension vibrations corresponding to the functional groups O-H of water and N-H of the physically absorbed  $\text{NH}_3$  [14]. Those bands around 1620  $\text{cm}^{-1}$  can be associated to the flexion modes of  $\text{H}_2\text{O}$  and  $\text{NH}_3$ . The band around 1380  $\text{cm}^{-1}$  on the other hand justifies the existence of M- $\text{NH}_3$  bonding as well as of the functional group  $\text{NO}_3^-$ , which can prompt the formation of different complexes during the process. On the other hand the sulphate ions also form numerous complexes and they can be distinguished from the tension modes of S-O bonding. In this way the broad band around 1140  $\text{cm}^{-1}$ , is evidence of the existence of  $\text{SO}_4^{2-}$  in the analyzed samples. Such a band shows a small shoulder around 1050  $\text{cm}^{-1}$  in the IR spectra corresponding to the first and fourth washed samples (Fig. 2(b)); this is indicative of a sulphate ion acting as an unidentate group ( $\text{C}_{3v}$ ) or as bidentate complex ( $\text{C}_{2v}$ ) [22]. However the small bands around 1019 and 1107  $\text{cm}^{-1}$  after the sixth washing now indicate that  $\text{SO}_4^{2-}$  behaves as an unidentate group and a free ion ( $\text{T}_d$ ) in the compound [22]. All these bands decreased in intensity with subsequent washings, which should be attributed only to the formation of the  $[\text{CH}_3\text{CH}_2]_2\text{NH}_2^+\text{HSO}_4^-$  ammonium salt which is soluble in water [23]. In the same way the band around 600  $\text{cm}^{-1}$  is associated with the vibration mode of  $\text{SO}_4^{2-}$ , but it is remarkable that all of these bands disappear after the

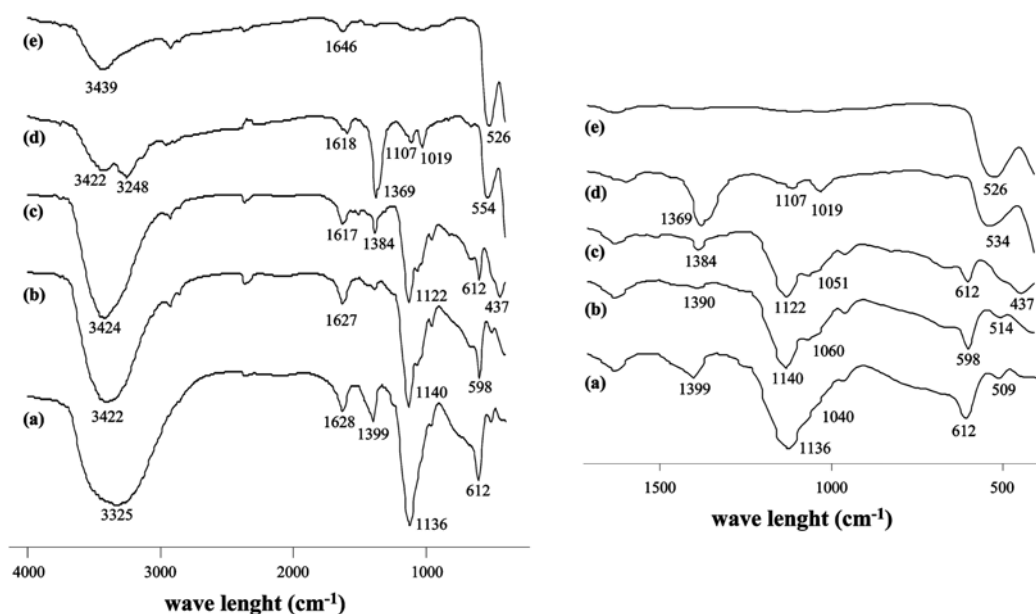


**Fig. 2.** Evolution of infrared spectra with ethylenediamine washing: a) unwashed as-obtained precipitate, b) first washing, c) fourth washing, d) sixth washing and e) eighth washing. On the left, zoom in of the shorter wave lengths.

**Table 1.** Evolution of representative IR bands (in  $\text{cm}^{-1}$ ) with the washing process

Unwashed precipitate	First washing	Fourth washing	Sixth washing	Eighth washing	Assignment
3325	3422	3424	3422 3248	3439	$\nu$ (OH), $\nu$ ( $\text{NH}_3$ )
1628	1627	1617	1618	1646	$\delta_d$ ( $\text{NH}_3$ ), ( $\text{H}_2\text{O}$ )
1399	1390	1384	1369	-	M- $\text{NH}_3$ , $\nu_3$ ( $\text{NO}_3$ )
1136	1140	1122	1107	-	$\nu_3$ ( $\text{SO}_4^{2-}$ ), $\nu_1$ ( $\text{NO}_3$ )
1040	1060	1051	1019	-	$\nu_4$ ( $\text{SO}_4^{2-}$ )
612	598	612	-	-	$\nu$ (Zn-O)
509	514	519	534	526	$\nu_2$ ( $\text{SO}_4^{2-}$ )
466	443	437	-	-	

eighth washing with ethylenediamine. This situation, points towards the formation of complexes of the type  $[\text{Zn}(\text{OH})_2]_3$  ( $\text{ZnSO}_4$ )( $\text{H}_2\text{O}$ )<sub>5</sub> which are highly soluble in ethylenediamine aqueous solutions. Finally the band around  $520 \text{ cm}^{-1}$  is associated with the Zn-O bonding and as can be observed it increases in intensity with the subsequent washings.

As long as the washing process proceeds, the conformed precipitates exhibit different crystalline phases. Fig. 3 shows the X-ray diffractograms for these solid samples. The first two spectra, corresponding to the unwashed solid and the solid obtained after the first washing with ethylenediamine, show poor crystallinity; nevertheless compounds like  $\text{Zn}_5(\text{NO}_3)_2(\text{OH})_8 \cdot 2\text{NH}_3$  (JCPDF file n° 45-5930) and  $\text{Zn}_4\text{SO}_4(\text{OH})_6 \cdot 4\text{H}_2\text{O}$  (JCPDF file n° 44-0673) can be detected evidencing the presence of complexes of  $\text{NO}_3^-$  and  $\text{SO}_4^{2-}$  as well as the physical absorption of  $\text{NH}_3$ . Identification of more compounds with XRD is hampered by the overlapping and low intensity of the different peaks, but even so, some of them match the patterns of phases such as  $\text{Zn}_4\text{SO}_4(\text{OH})_6 \cdot 5\text{H}_2\text{O}$  (JCPDF file n° 39-0688),  $(\text{Zn}(\text{OH})_2)_3(\text{ZnSO}_4)(\text{H}_2\text{O})_5$  (JCPDF file n° 78-0246) and  $\text{ZnSO}_4(\text{NH}_4)_2\text{SO}_4 \cdot 6\text{H}_2\text{O}$  (JCPDF file

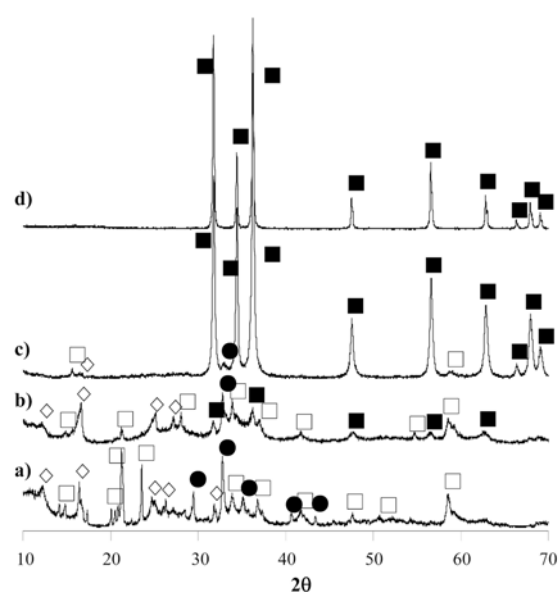


**Fig. 3.** Evolution of X-Ray diffraction patterns with ethylenediamine washing: a) as-obtained precipitate, b) first washing, c) fourth washing and d) eighth washing. ■ ZnO, ◇  $[\text{Zn}(\text{OH})_2]_3(\text{ZnSO}_4)(\text{H}_2\text{O})_5$ , □  $\text{Zn}_4(\text{SO}_4)(\text{OH})_6 \cdot 4\text{H}_2\text{O}$  and ●  $\text{ZnSO}_4(\text{NH}_4)_2\text{SO}_4 \cdot 6\text{H}_2\text{O}$ .

n° 01-0414). Also, the first peaks of the ZnO phase (JCPDF file n° 27-0985) are observed after this first washing. Increasing the number of washing steps leads to a higher degree of crystallinity as can be observed in the diffractograms. More specifically after the fourth washing, Fig. 3(c), the basic zinc sulphates are practically removed from the solid sample, leading to a pure ZnO single phase after washing eight times with ethylenediamine.

Transmission electron microscopy was finally employed for a further investigation of the particles morphology and composition. In this way Fig. 4 shows the evolution of the microstructure with the washing process as followed by TEM. Big agglomerates of particles with irregular shapes and sizes are observed in the as-obtained unwashed solid and the situation does not change substantially after four washing steps (Fig. 4(a)). However after the sixth washing step, the agglomeration starts to decrease and the first crystals with an acicular-like shape can be observed (Fig. 4(b)). Finally after washing eight times with ethylenediamine every particle shows a characteristic needle morphology (Fig. 4(c)). As inferred from the micrograph the needles exhibit a nanometric diameter (below 100 nm wide) and they are several micrometers in length. EDS of these particles gives evidence of the complete absence of any trace of impurities in the ZnO powder obtained.

To summarize, the controlled precipitation method is found to be suitable to produce high purity zinc oxide nanoneedles at room temperature. Titration curves showed three different zones during the addition of  $\text{NH}_4\text{OH}$  to the solution of the sulphate precursor. The main reactions in zone I involve the neutralization of the acidic complexes as well as the hydrolysis of the aqueous species. Polycondensation reactions occur in zone II and the formation of zincates in zone III. During the synthesis process, the as-formed precipitate undergoes phase transformations. Initially it is composed by nitrate and sulphate like complexes. However the counterions can be removed by subsequent washings with ethylenediamine leading finally to pure zinc oxide of nanometric size and needle type morphology.

## Conclusions

During the synthesis of zinc oxide nanoparticles by the controlled precipitation method, chemical weathering and solution processes take place and can be controlled by acting on the solution concentration, pH and washing medium. Recrystallization of these nanoparticles leads to different phase transformations between different zinc complexes. When using acetate as a precursor of zinc, the washing step with ethanol does not complete the transformation to pure ZnO and additional thermal treatments are required. On the other hand the use of a sulphate precursor requires less ammonia to precipitate the solid and the use of ethylenediamine as the washing agent leads to a complete decomposition of the intermediate sulphate

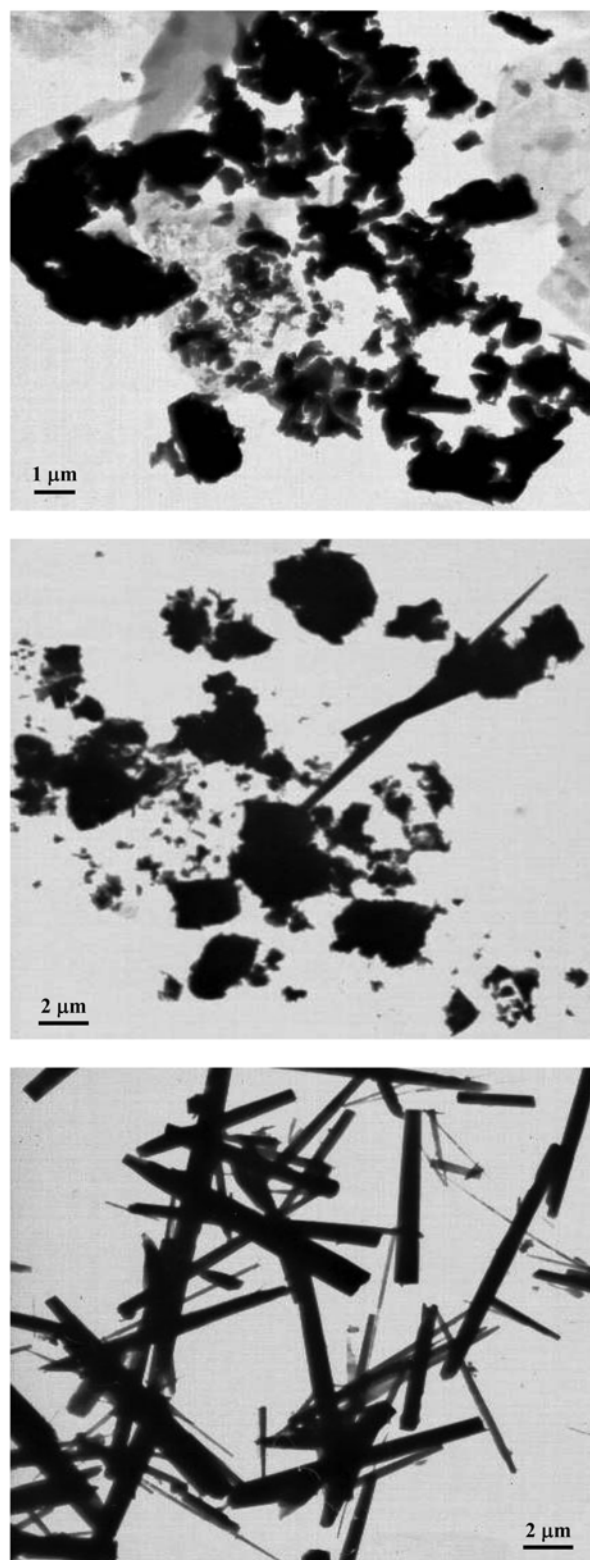


**Fig. 4.** Evolution of ZnO particle morphology with washing steps as followed by TEM: a) fourth washing, b) sixth washing and c) eighth washing.

complexes, and a complete transformation to ZnO can be achieved at room temperature.

## References

1. S.J. Pearton, D.P. Norton, K. Ip, Y.W. Heo and T. Steiner, *Prog. Mater. Sci.* 50[3] (2005) 293-340.
2. M. Peiteado, *Bol. Soc. Esp. Ceram. V.* 44[2] (2005) 77-87.
3. D.C. Look, *Mater. Sci. Eng. B-Solid.* 80[1-3] (2001) 383-387.
4. S.A. Wolf, D.D. Awschalom, R.A. Buhrman, J.M. Daughton, S. von Molnar, M.L. Roukes, A.Y. Chtchelkanova and D.M. Treger, *Science* 294[5546] (2001) 1488-1495.
5. X.H. Sun, S. Lam, T.K. Sham, F. Heigl, A. Jürgensen and N.B. Wong, *J. Phys. Chem. B.* 109[8] (2005) 3120-3125.
6. Y.J. Kwon, K.H. Kim, C.S. Lim and K.B. Shim, *J. Ceram. Process. Res.* 3[3] (2002) 146-149.
7. X.D. Gao, X.M. Li and W.D. Yu, *J. Solid State Chem.* 178[4] (2005) 1139-1144.
8. X.Y. Zhang, J.Y. Dai, C.H. Lam, H.T. Wang, P.A. Webley, Q. Li and H.C. Ong, *Acta Mater.* 55[15] (2007) 5039-5044.
9. H. Tanaka, A. Fujioka, A. Futoyu, K. Kandori and T. Ishikawa, *J. Solid State Chem.* 180[7] (2007) 2061-2066.
10. H. Zhou and Z. Li, *Mater. Chem. Phys.* 89[2-3] (2005) 326-331.
11. Z. Gui, X. Wang, J. Liu, S.S. Yan, Y.Y. Ding, Z.Z. Wang and Y. Hu, *J. Solid State Chem.* 179[7] (2006) 1984-1989.
12. S.H. Yoon, H. Yang and Y.S. Kim, *J. Ceram. Process. Res.* 8[4] (2007) 261-265.
13. P. Tonto, O. Mekasuwandumrong, S. Phatanasri, V. Pavarajarn and P. Praserttham, *Ceram. Int.* 34[1] (2008) 57-62.
14. W.A. Deheer, A. Chatelain and D. Ugarte, *Science* 270 [5239](1995) 1179-1180.
15. E.J.A. Campo, H. Aristizabal and J.E. Rodríguez-Páez, *Bol. Soc. Esp. Ceram. V.* 45[4] (2006) 283-288.
16. W. Lee, M.C. Jeong and J.M. Myoung, *Acta Mater.* 52[13] (2004) 3949-3957.
17. M. Yang, G.S. Pang, L.F. Jiang and S.H. Feng, *Nanotechnology* 17[1] (2006) 206-212.
18. J.J. Chen, M.H. Yu, W.L. Zhou, K. Sun and L.M. Wang, *Appl. Phys. Lett.* 87[17] (2005) 173119.
19. S. Chakrabarti and S. Chaudhuri, *Mater. Chem. Phys.* 87[1] (2004) 196-200.
20. T. Masaki, S.J. Kim, H. Watanabe, K. Miyamoto, M. Ohno and K.H. Kim, *J. Ceram. Process. Res.* 4[3] (2003) 135-139.
21. J.E. Rodríguez-Páez, A.C. Caballero, M. Villegas, C. Moure, P. Durán and J.F. Fernández, *J. Eur. Ceram. Soc.* 21[7] (2001) 925-930.
22. K. Nakamoto, in "Infrared and Raman spectra of inorganic and coordination compounds. Part B: Applications in coordination, organometallic and bioinorganic chemistry" (John Wiley & Sons, New York, 1997) p. 79.
23. T.W. Graham Solomons, in "Organic Chemistry" (John Wiley & Sons, New York, 1992) p.834.